Supplemental information for:

Incorporation of pendant bases into Rh(diphosphine)$_2$ complexes: Synthesis, thermodynamic studies, and catalytic CO_2 hydrogenation activity of $[Rh(P_2N_2)_2]^+$ complexes

Alyssia M. Lilio[a], Mark Reineke[a], Curtis E. Moore[a], Arnold L. Rheingold[a], Michael K. Takase[b], and Clifford P. Kubiak[a]*

[a]Department of Chemistry and Biochemistry, University of California San Diego, 9500 Gilman Drive MC 0358, La Jolla, California 92093, United States

[b]Beckman Institute, California Institute of Technology, 1200 E. California Blvd., Caltech MC 139-74, Pasadena, CA 91125

Table of Contents **Page**

Table 1. ^{1}H and $^{31}P\{^{1}H\}$ NMR assignments for $[Rh(P_2N_2)_2]^+$, $HRh(P_2N_2)_2$, and $[H_2Rh(P_2N_2)_2]^+$ complexes

Complex		$^{31}P\{^{1}H\}$NMR (ppm)	^{1}H NMR hydride peak (ppm)
1	$[Rh(P^{Ph}{}_2N^{Ph}{}_2)_2]^+$	5.38[a]	—
2	$[Rh(P^{Ph}{}_2N^{Bn}{}_2)_2]^+$	–2.71[a]	—
3	$[Rh(P^{Ph}{}_2N^{PhOMe}{}_2)_2]^+$	3.87[a]	—
4	$[Rh(P^{Cy}{}_2N^{Ph}{}_2)_2]^+$	9.6[a]	—
5	$[Rh(P^{Cy}{}_2N^{PhOMe}{}_2)_2]^+$	8.09[a]	—
6	$HRh(P^{Ph}{}_2N^{Ph}{}_2)_2$	16.06[b]	–8.43[b]
7	$HRh(P^{Ph}{}_2N^{Bn}{}_2)_2$	9.05[b]	–7.66[b]
8	$HRh(P^{Ph}{}_2N^{PhOMe}{}_2)_2$	13.79[b]	–8.32[b]
9	$HRh(P^{Cy}{}_2N^{Ph}{}_2)_2$	21.72[b]	–10.27[b]
10	$HRh(P^{Cy}{}_2N^{PhOMe}{}_2)_2$	21.67[b]	–10.20[b]
	$[H_2Rh(P^{Ph}{}_2N^{Ph}{}_2)_2]^+$	15.25, 1.79[b]	[c]
	$[H_2Rh(P^{Ph}{}_2N^{Bn}{}_2)_2]^+$	12.38, 2.97[b]	[c]
	$[H_2Rh(P^{Ph}{}_2N^{PhOMe}{}_2)_2]^+$	13.3, 1.12[b]	[c]
	$[H_2Rh(P^{Cy}{}_2N^{Ph}{}_2)_2]^+$	15.99, 16.54[b]	[c]
	$[H_2Rh(P^{Cy}{}_2N^{PhOMe}{}_2)_2]^+$	15.22, 14.61[b]	[c]

[a]Spectra recorded in CD_3CN. [b]Spectra recorded in C_6D_6. [c]Not observed.

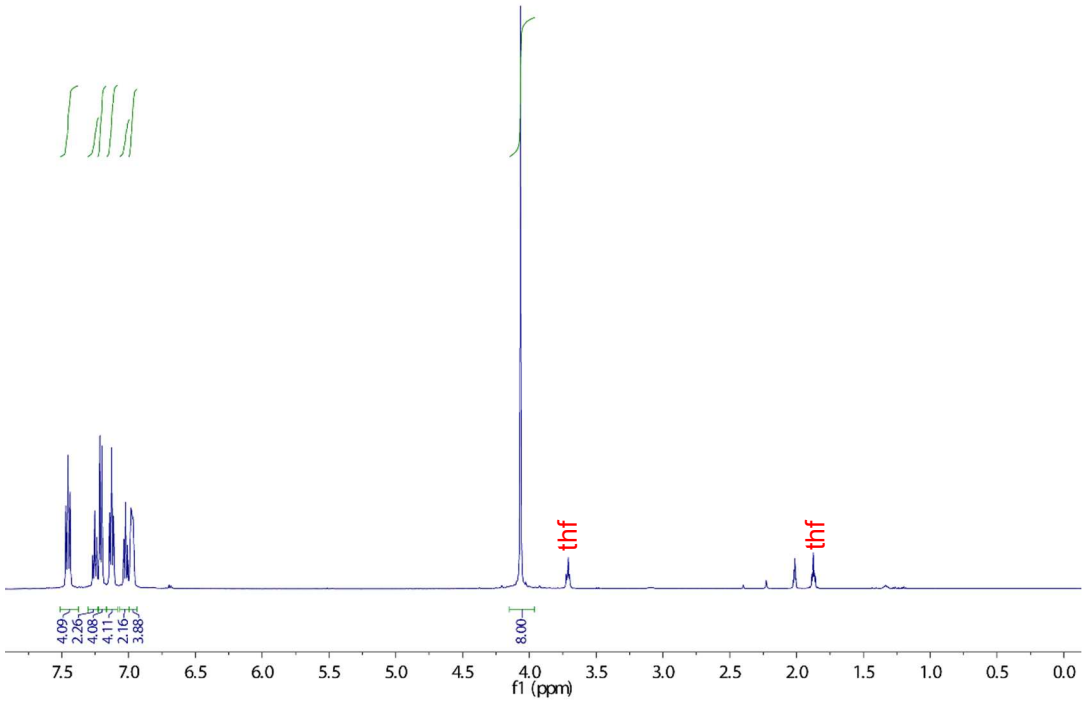

Figure 1. ^{1}H NMR (500 MHz) of $[Rh(P^{Ph}{}_2N^{Ph}{}_2)_2]BF_4$ (**1**) in CD_3CN.

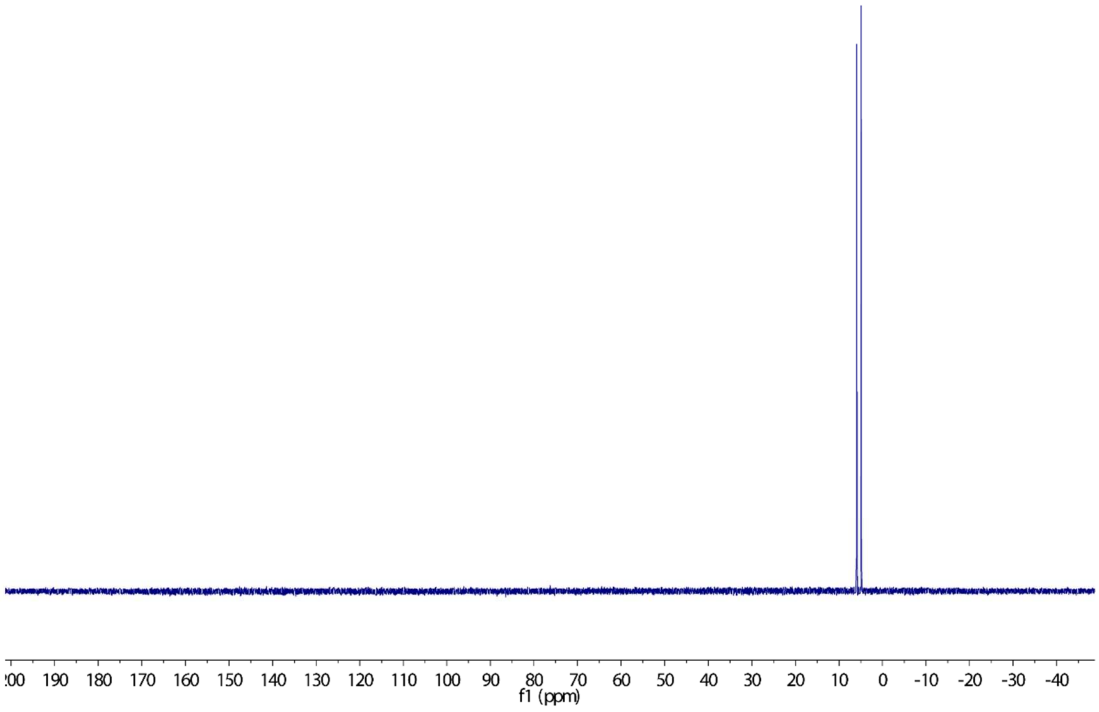

Figure 2. $^{31}P\{^{1}H\}$ NMR (121 MHz) of $[Rh(P^{Ph}{}_2N^{Ph}{}_2)_2]BF_4$ (**1**) in CD_3CN.

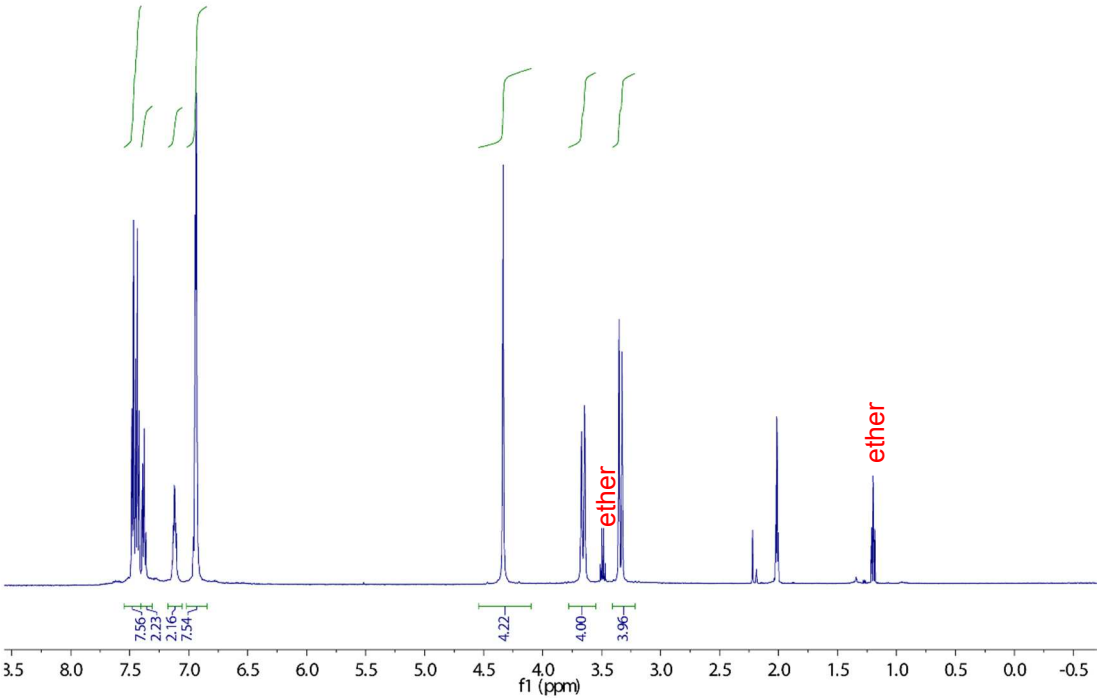

Figure 3. ^{1}H NMR (500 MHz) of [Rh($P^{Ph}_2N^{Bn}_2$)$_2$]BF_4 (**2**) in CD_3CN.

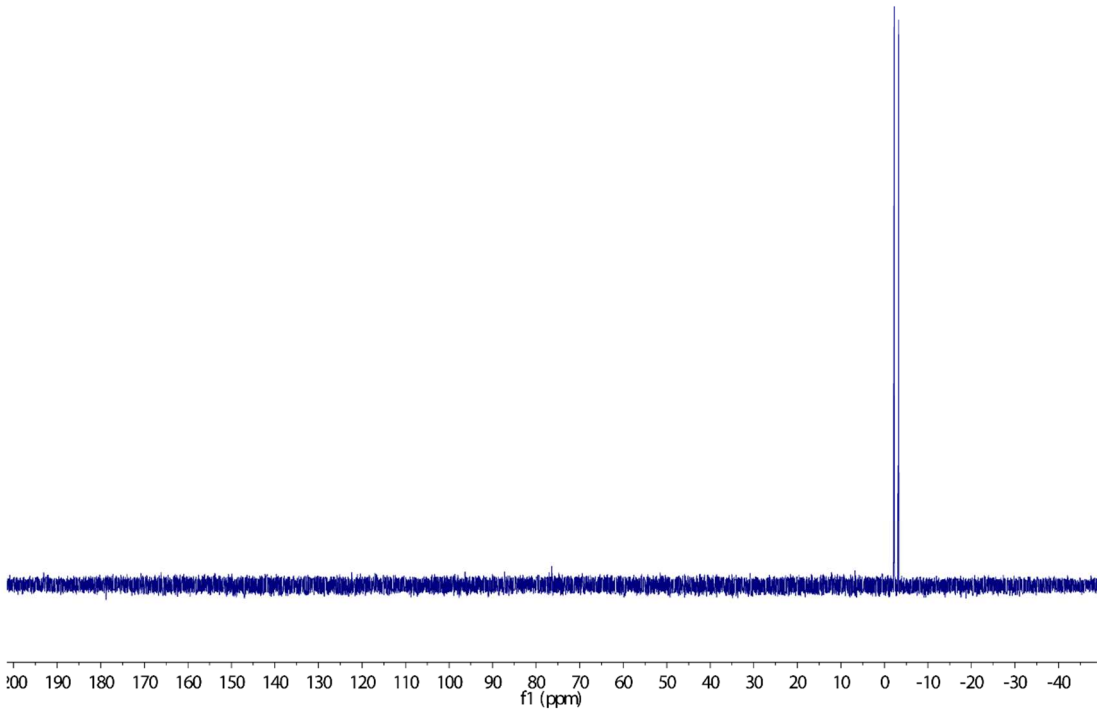

Figure 4. ^{31}P{^{1}H} NMR (121 MHz) of [Rh($P^{Ph}_2N^{Bn}_2$)$_2$]BF_4 (**2**) in CD_3CN.

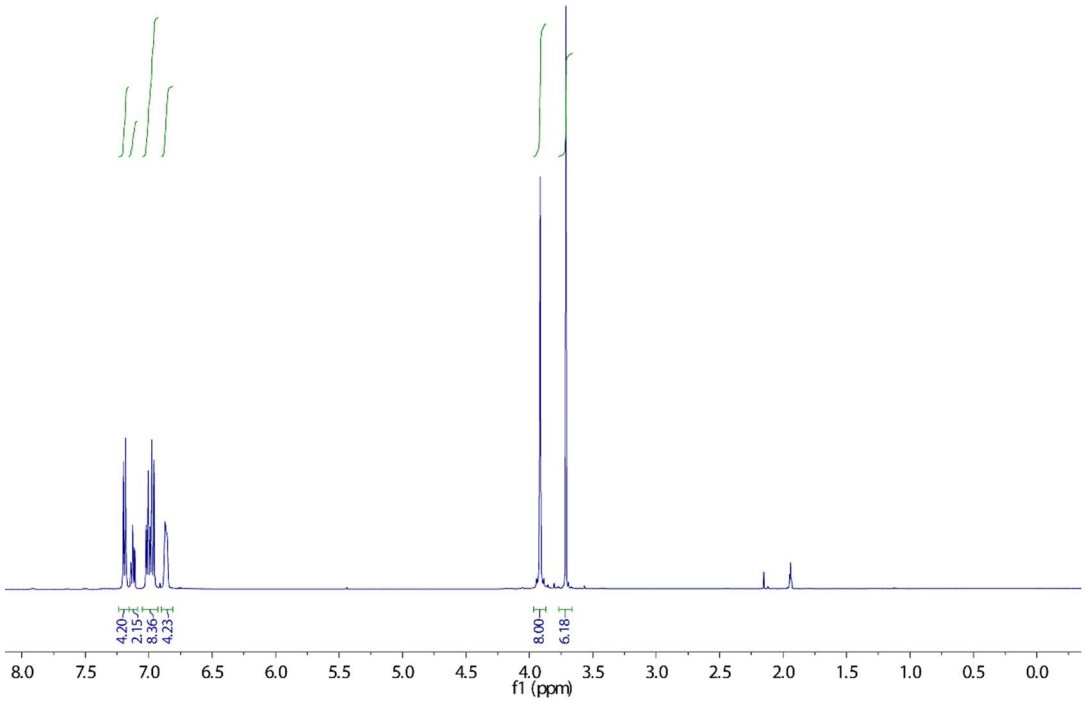

Figure 5. ^{1}H NMR (500 MHz) of [Rh($P^{Ph}_2N^{PhOMe}_2$)$_2$]BF_4 (**3**) in CD_3CN.

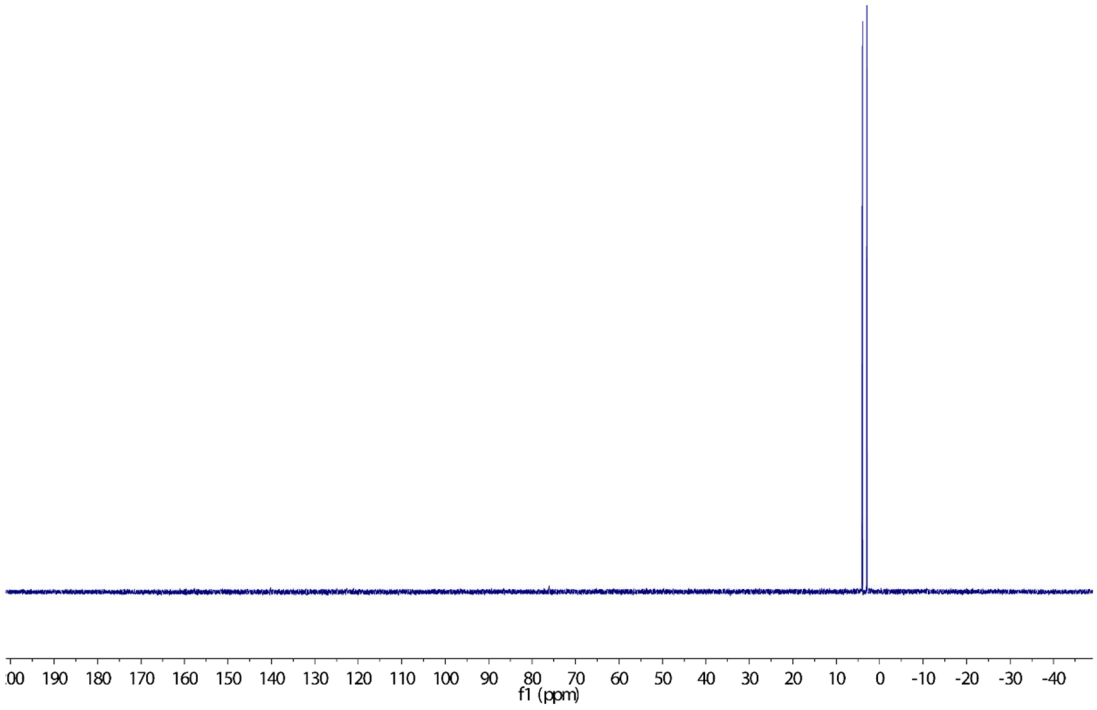

Figure 6. $^{31}P\{^{1}H\}$ NMR (121 MHz) of [Rh($P^{Ph}_2N^{PhOMe}_2$)$_2$]BF_4 (**3**) in CD_3CN.

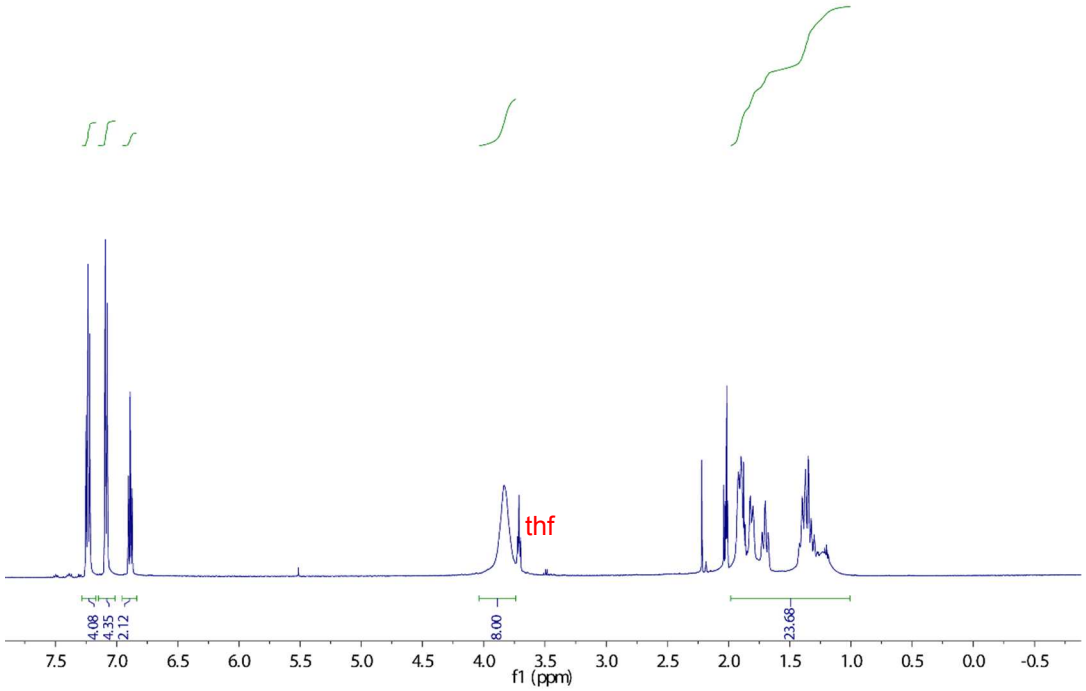

Figure 7. ^{1}H NMR (500 MHz) of [Rh($P^{Cy}_2N^{Ph}_2$)$_2$]BF_4 (**4**) in CD_3CN.

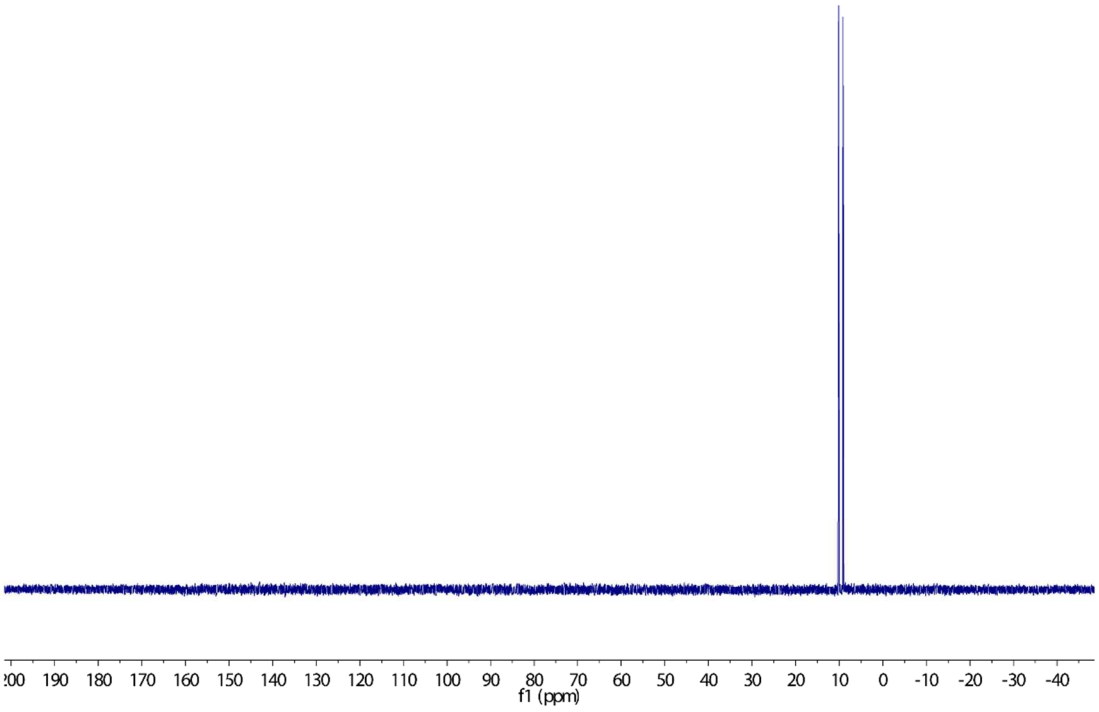

Figure 8. $^{31}P\{^{1}H\}$ NMR (121 MHz) of [Rh($P^{Cy}_2N^{Ph}_2$)$_2$]BF_4 (**4**) in CD_3CN.

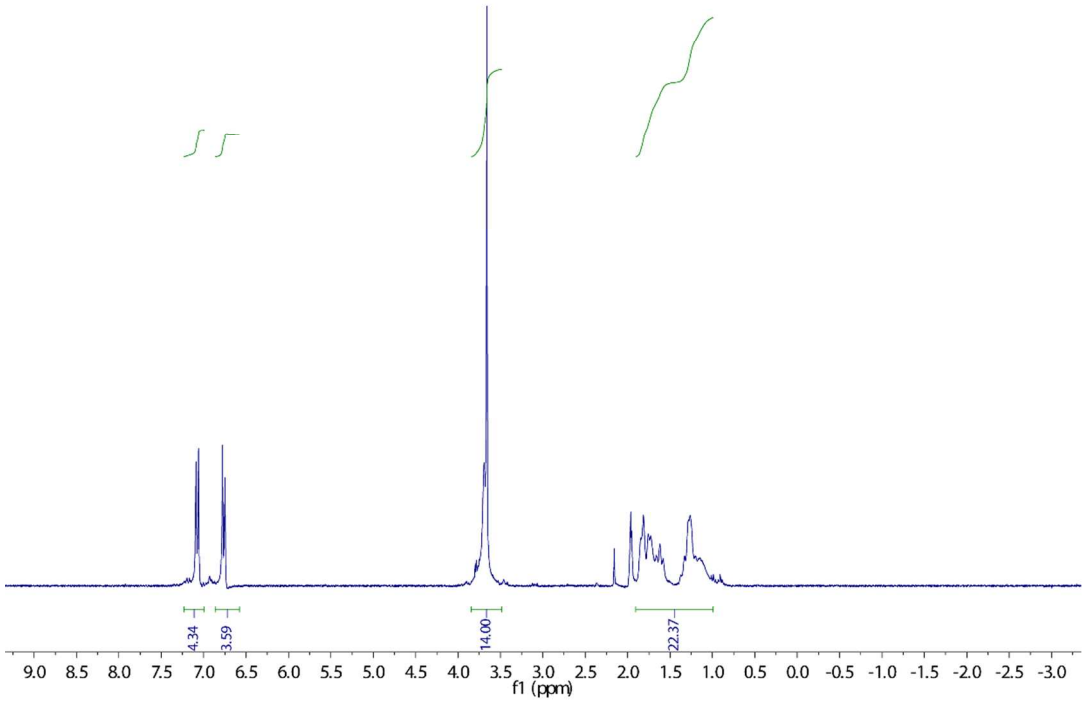

Figure 9. ^{1}H NMR (300 MHz) of $[Rh(P^{Cy}{}_2N^{PhOMe})_2]BF_4$ (**5**) in CD_3CN.

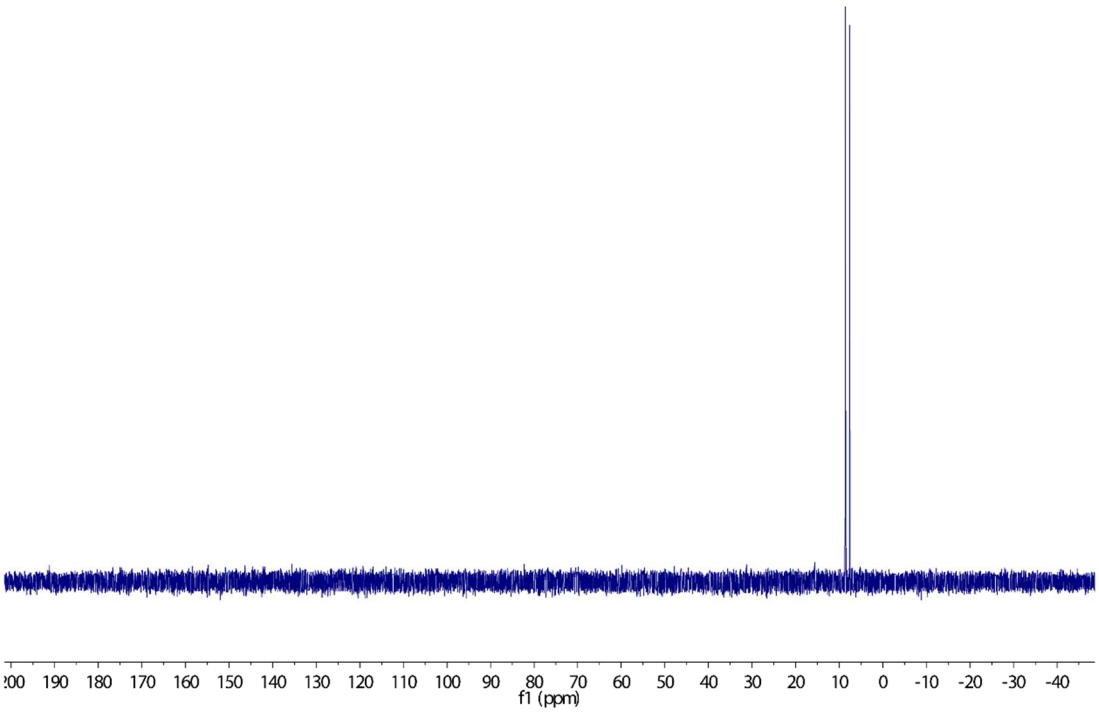

Figure 10. $^{31}P\{^{1}H\}$ NMR (121 MHz) of $[Rh(P^{Cy}{}_2N^{PhOMe}{}_2)_2]BF_4$ (**5**) in CD_3CN.

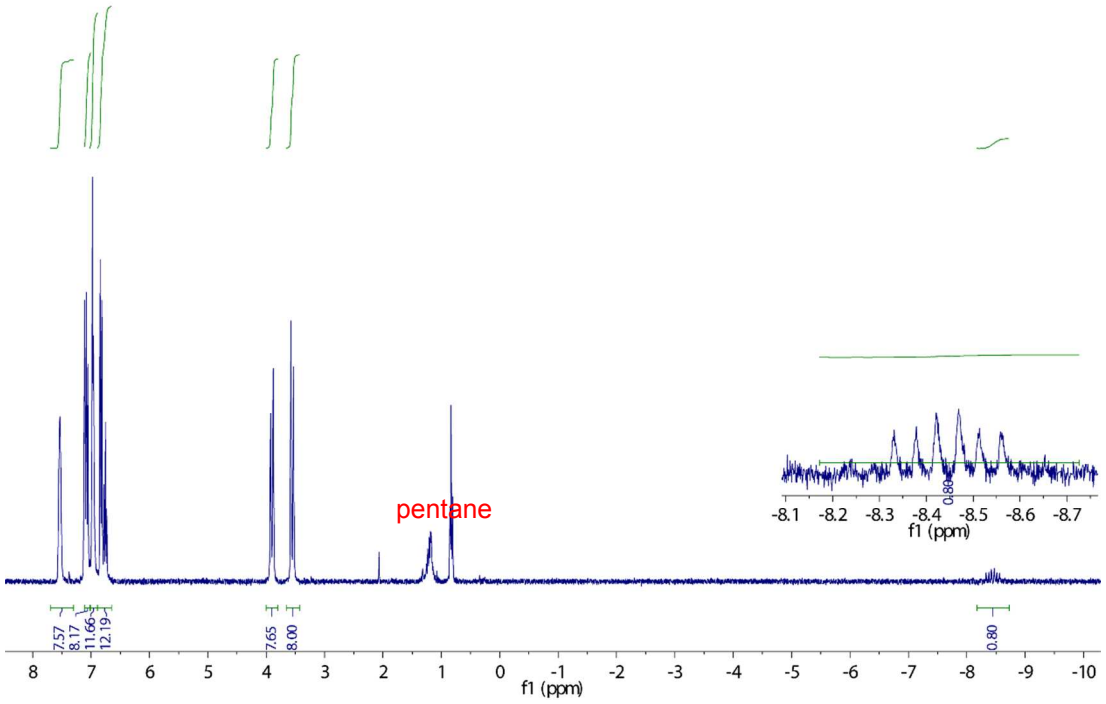

Figure 11. ^{1}H NMR (500 MHz) of HRh($P^{Ph}_2N^{Ph}_2$)$_2$ (**6**) in C_6D_6.

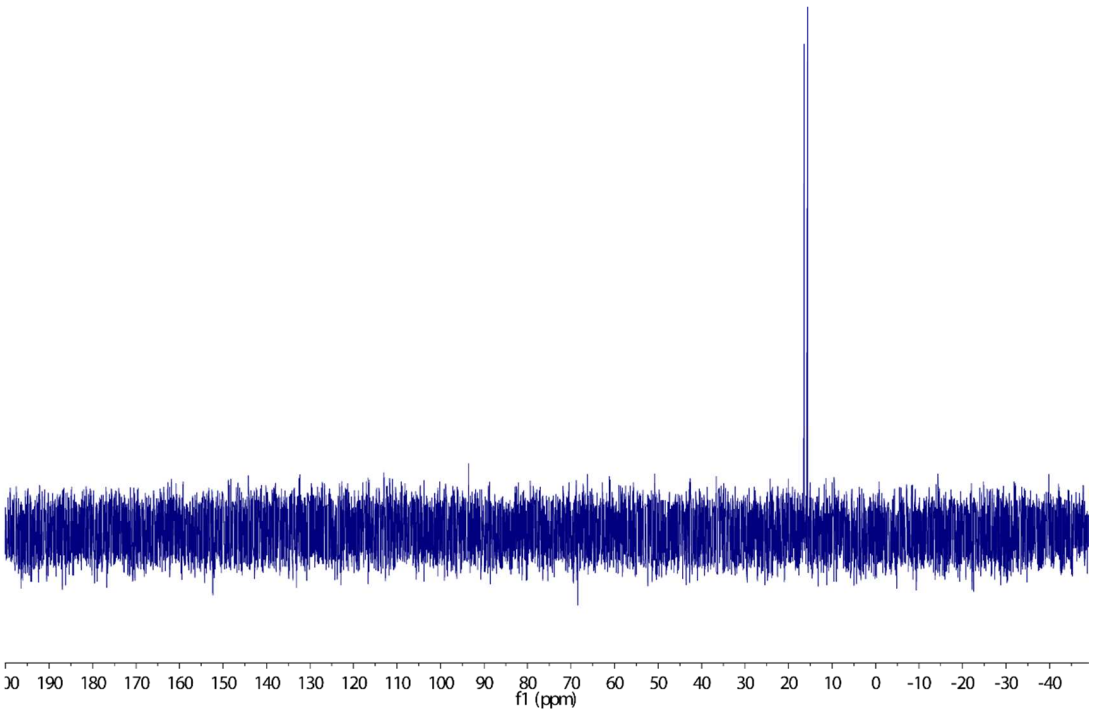

Figure 12. ^{31}P{^{1}H}NMR (121 MHz) of HRh($P^{Ph}_2N^{Ph}_2$)$_2$ (**6**) in C_6D_6.

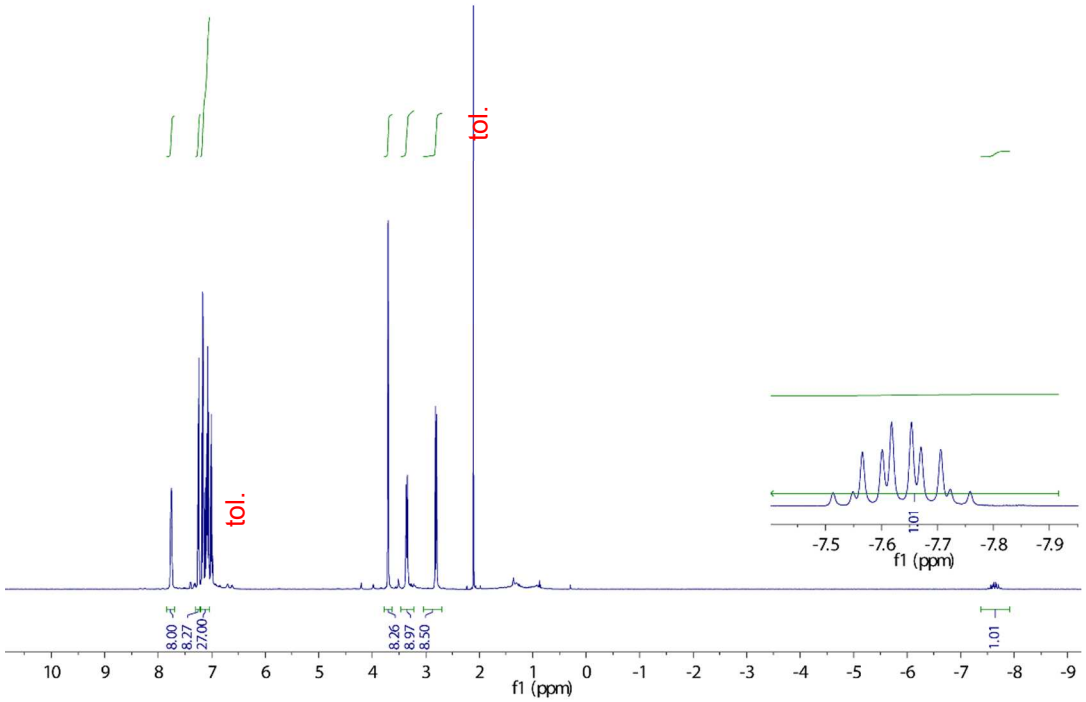

Figure 13. ^{1}H NMR (500 MHz) of HRh($P^{Ph}_2N^{Bn}_2$)$_2$ (**7**) in C_6D_6.

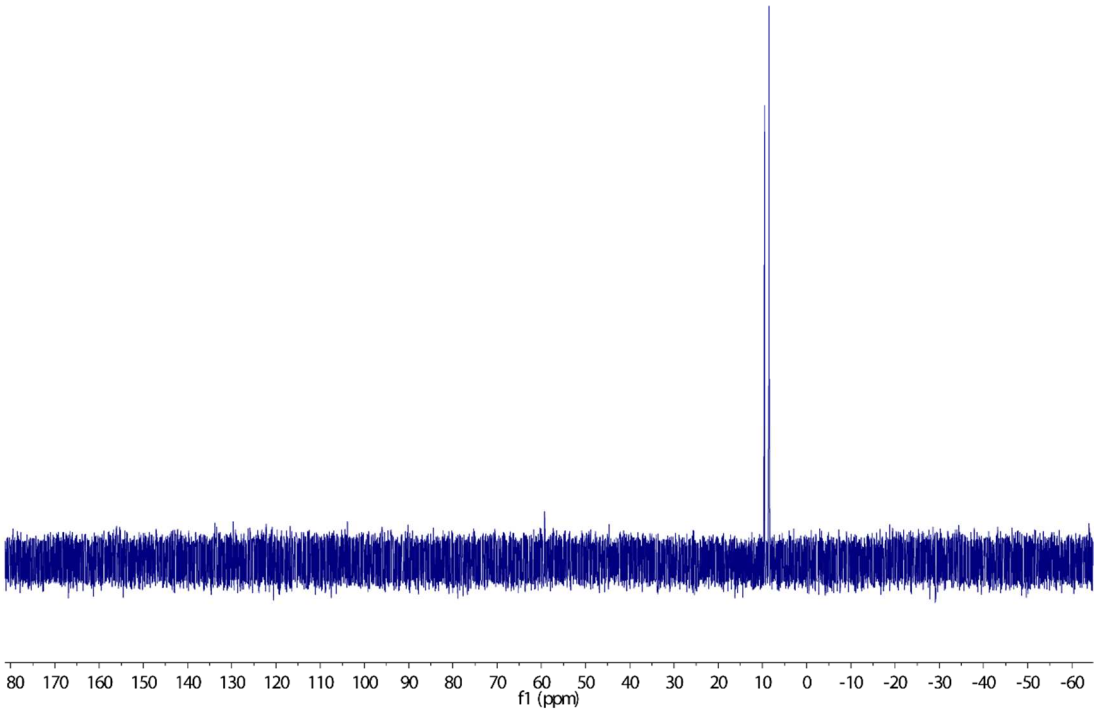

Figure 14. ^{31}P{^{1}H} NMR (121 MHz) of HRh($P^{Ph}_2N^{Bn}_2$)$_2$ (**7**) in C_6D_6.

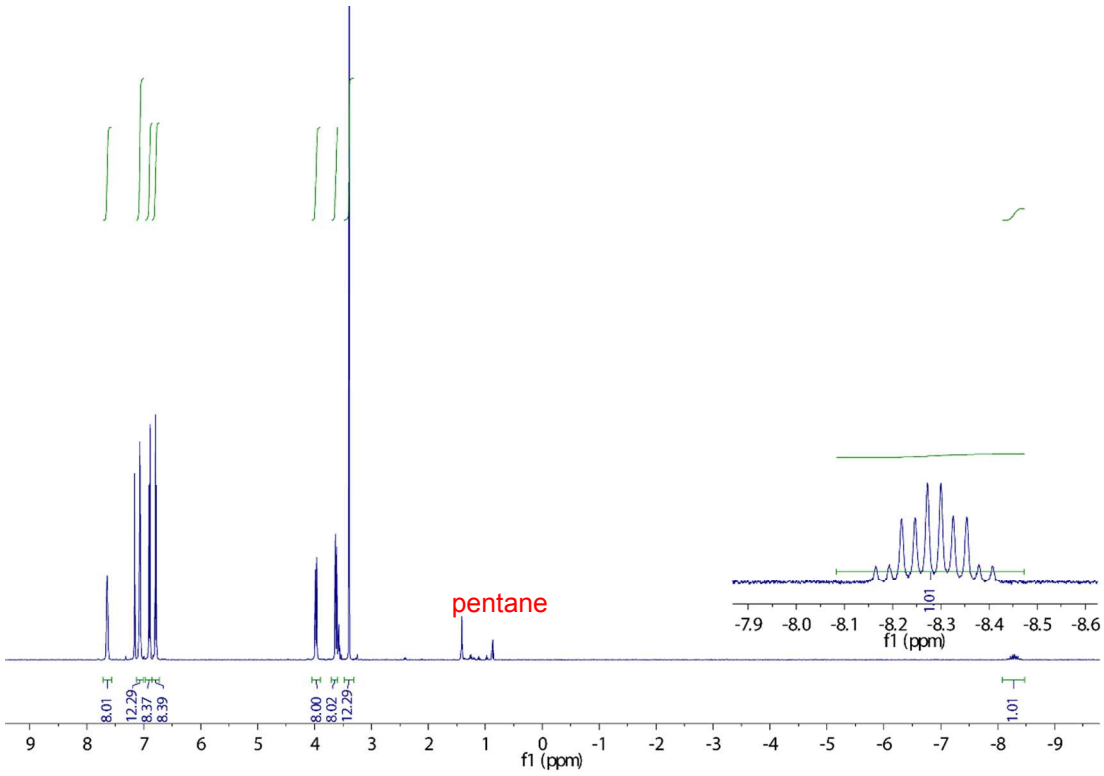

Figure 15. ^{1}H NMR (500 MHz) of HRh($P^{Ph}_2N^{PhOMe}_2$)$_2$ (**8**) in C_6D_6.

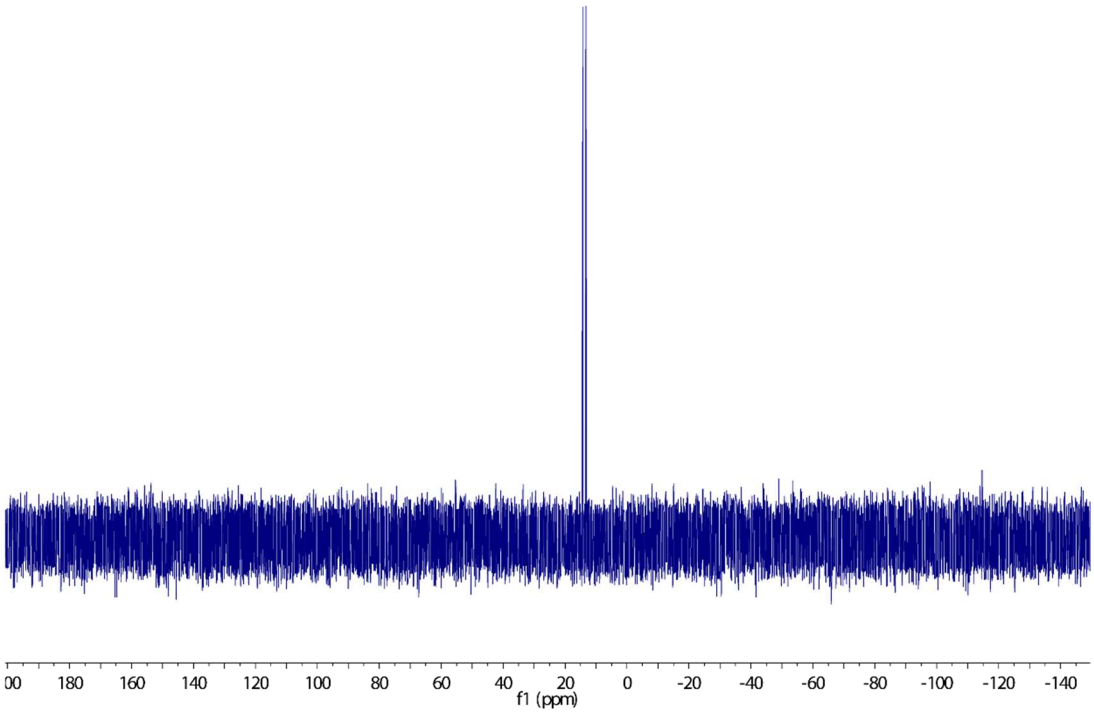

Figure 16. ^{31}P{^{1}H}NMR (121 MHz) of HRh($P^{Ph}_2N^{PhOMe}_2$)$_2$ (**8**) in C_6D_6.

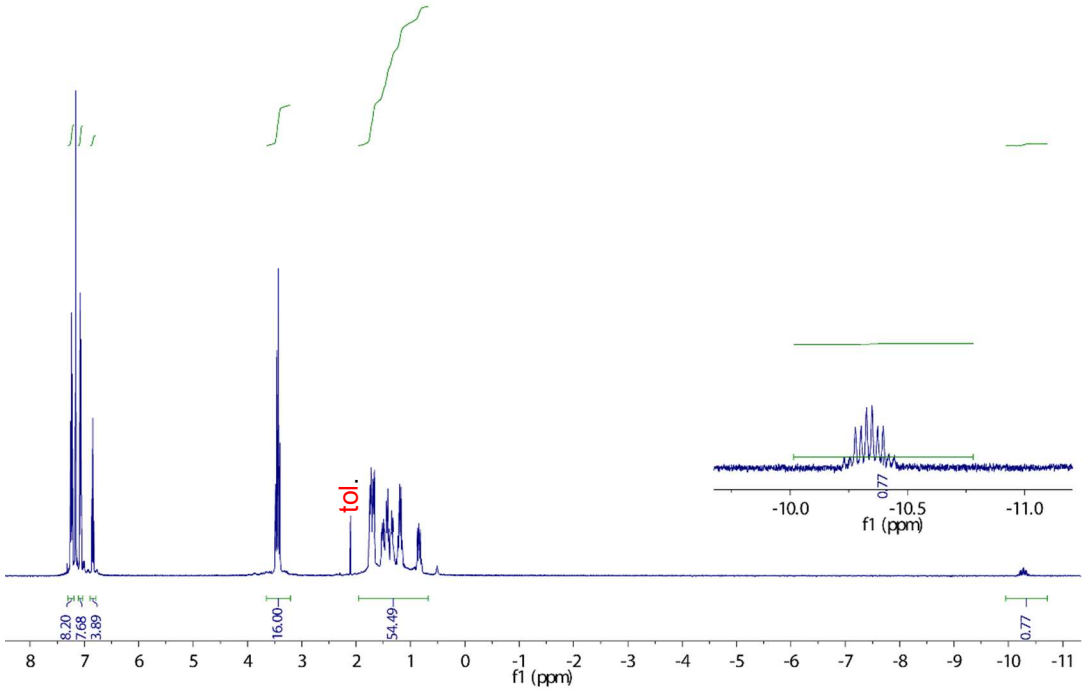

Figure 17. ^{1}H NMR (500 MHz) of HRh($P^{Cy}_2N^{Ph}_2$)$_2$ (**9**) in C_6D_6.

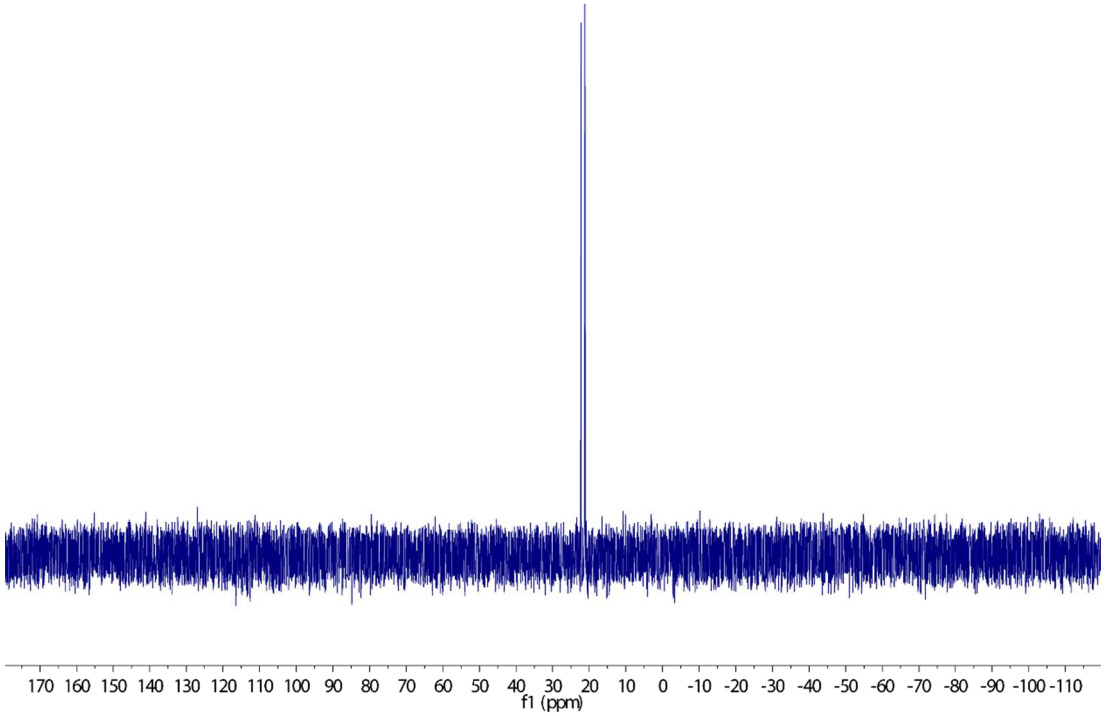

Figure 18. ^{31}P{^{1}H} NMR (121 MHz) of HRh($P^{Cy}_2N^{Ph}_2$)$_2$ (**9**) in C_6D_6.

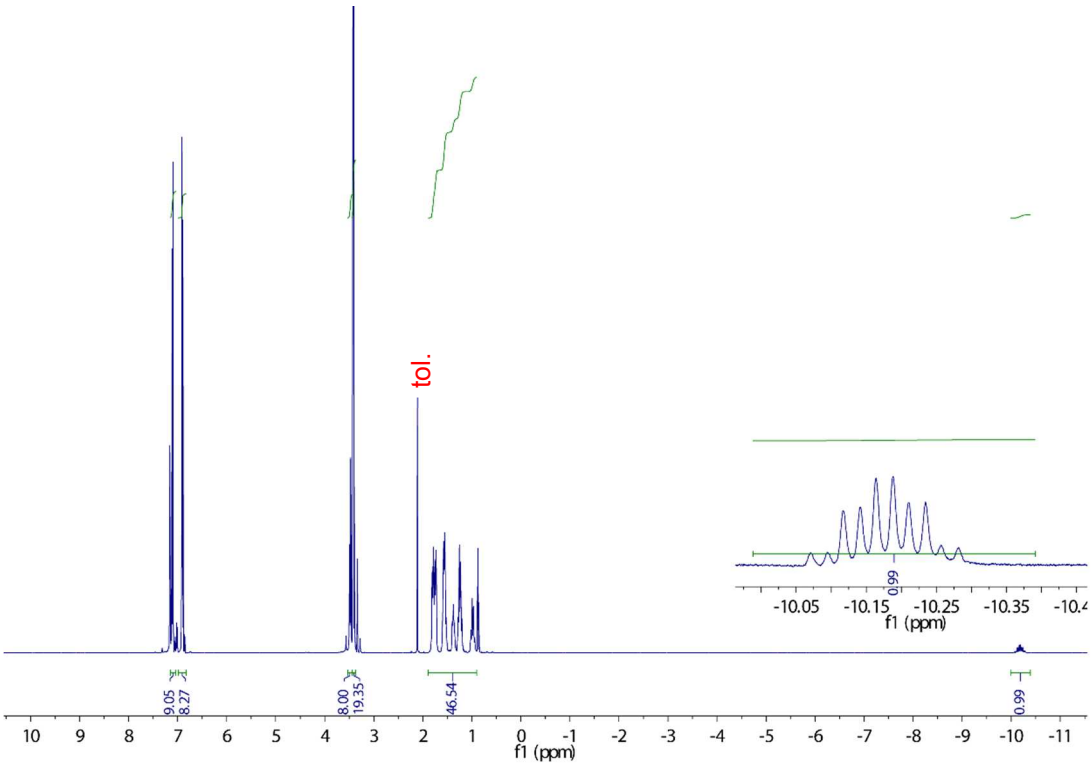

Figure 19. ^{1}H NMR (500 MHz) of HRh($P^{Cy}_2N^{PhOMe}_2$)$_2$ (**10**) in C_6D_6.

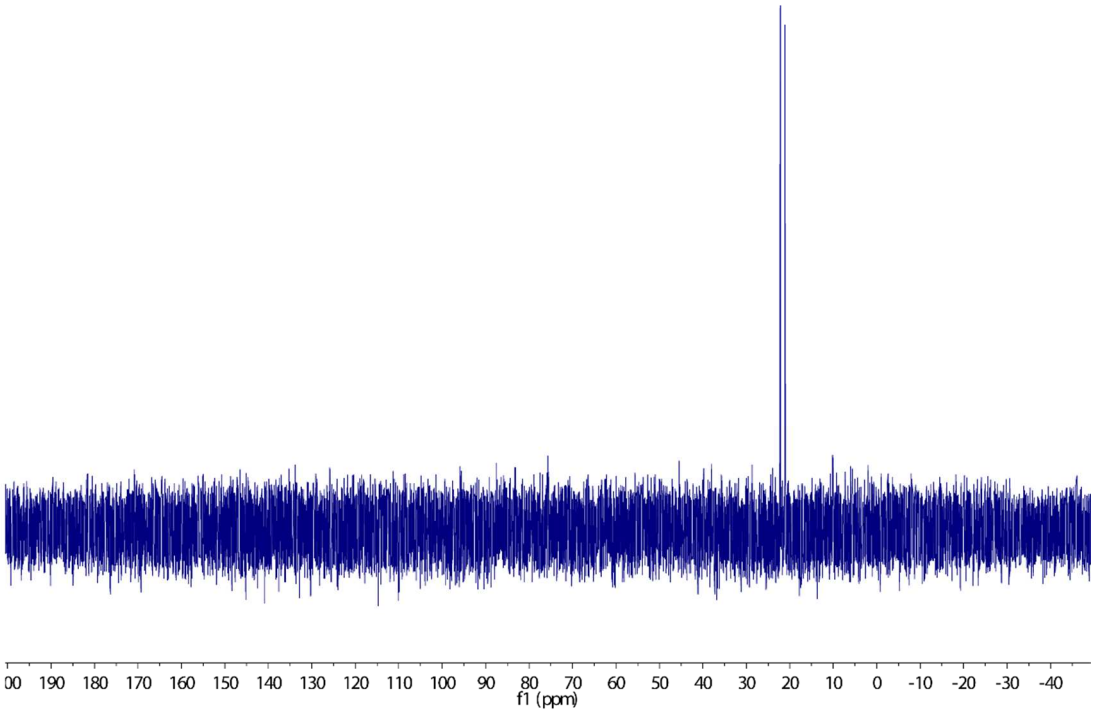

Figure 20. ^{31}P{^{1}H} NMR (121 MHz) of HRh($P^{Cy}_2N^{PhOMe}_2$)$_2$ (**10**) in C_6D_6.

Table 2. Crystallographic data and refinement information

	$[Rh(P^{Ph}{}_2N^{Ph}{}_2)_2]PF_6$	$[Rh(P^{Ph}{}_2N^{Bn}{}_2)_2]BF_4$	$[Rh(P^{Ph}{}_2N^{PhOMe}{}_2)_2]BF_4$	$[Rh(P^{Cy}{}_2N^{Ph}{}_2)_2]BF_4$
empirical formula	$C_{59}H_{57}F_6N_{2.5}P_5Rh$	$C_{62}H_{69}BF_4N_4O_{0.5}P_4Rh$	$C_{62}H_{67}BF_4N_5O_4P_4Rh$	$C_{56}H_{80}BF_4N_4P_4Rh$
formula weight	1172.83	1180.04	1106.64	1102.84
temperature (K)	100(2)	100(2)	100(2)	100(2)
wavelength Å	1.54178	0.71073	0.71073	0.71073
crystal system	Monoclinic	Triclinic	Monoclinic	Monoclinic
Spacegroup	P21/n	P-1	$P2_1/c$	$P2_1/n$
a (Å)	16.0883(4)	10.3561(4)	12.8250(11)	10.0583(10)
b (Å)	17.7264(5)	22.3066(9)	17.1647(16)	23.787(3)
c (Å)	18.4436(5)	25.1180(11)	26.185(2)	23.004(2)
α (°)	90	78.3650(10)	90	90
β (^{0})	98.3280(10)	78.3650(10)	94.522(4)	93.350(2)
γ (^{0})	90	85.9470(10	90	90
volume (Å^3)	5204.4(2)	5668.9(4)	5746.3(9)	5494.4(10)
Z	4	4	4	4
density	1.497	1.383	1.279	1.357
2θ range (°)	3.41 to 70.64	0.934 to 25.410	1.42 to 26.45	1.23 to 28.32
R(F), *R*w(F) (all data)	0.0405, 0.1069	0.0765, 0.1060	0.0757, 0.1151	0.0955, 0.1378
	$[Rh(P^{Cy}{}_2N^{PhOMe}{}_2)_2]BF_4$	$HRh(P^{Ph}{}_2N^{Bn}{}_2)_2$	$HRh(P^{Ph}{}_2N^{PhOMe}{}_2)_2$	$HRh(P^{Cy}{}_2N^{Ph}{}_2)_2$
empirical formula	$C_{64}H_{94}BF_4N_6O_4P_4Rh$	$C_{60}H_{65}N_4P_4Rh$	$C_{64}H_{73}N_4O_5P_4Rh$	$C_{56}H_{81}N_4P_4Rh$
formula weight	1325.05	1068.95	1205.05	1037.03
temperature (K)	100(2)	100(2)	100(2)	100(2)
wavelength Å	0.71073	0.71073	0.71073	0.71073
crystal system	monoclinic	Triclinic	monoclinic	tetragonal
spacegroup	C2/c	P-1	P 1 21 1	I-4
a (Å)	22.7509(9)	10.0167(7)	9.9890(2)	22.764(7)
b (Å)	13.4975(6)	14.2416(9)	48.2896(9)	22.7640(7)
c (Å)	22.3982(9)	18.7726(12)	12.8422(3)	20.1397(5)
α (°)	90	96.498(2)	90	90
β (^{0})	109.6649(15)	90.811(3)	112.6250(10)	90
γ (^{0})	90	100.226(3)	90	90
volume (Å^3)	6476.9(5)	2616.8(3)	5717.9(2)	10436.4
Z	4	2	4	8
density	1.359	1.357	1.400	1.320
2θ range (°)	2.207 to 36.394	1.463 to 36.387	1.687 to 26.000	2.242 to 27.491
R(F), *R*w(F) (all data)	0.1046 (0.0984)	0.0420 (0.0747)	0.0257 (0.0582)	0.0573 (0.1035)

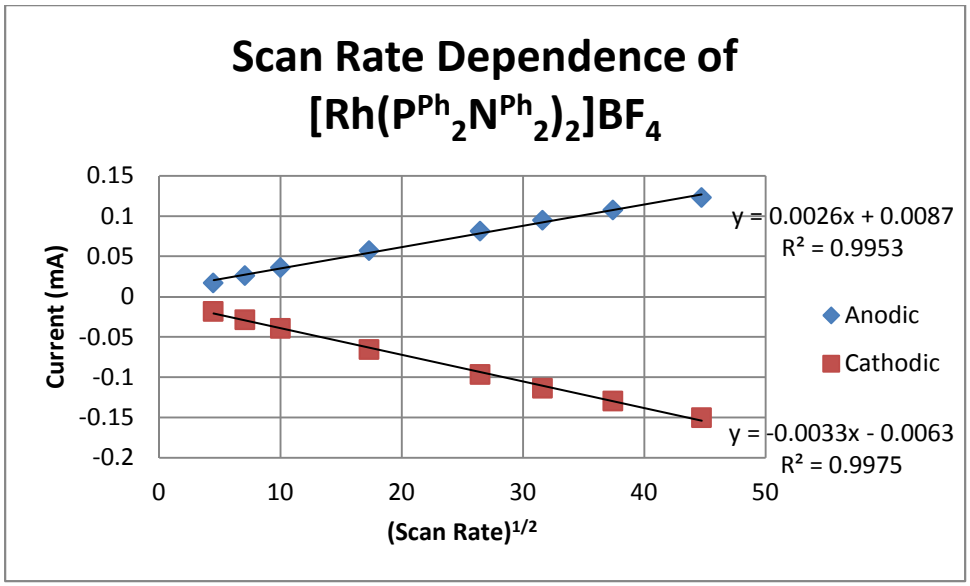

Figure 21. Scan rate dependence study of the Rh(1/-1) couple of 1 mM [Rh($^{Ph}_2N^{Ph}_2$)$_2$]BF_4 (**1**). Conditions: 0.1 M NBu_4PF_6 in acetonitrile, glassy carbon working and counter electrodes.

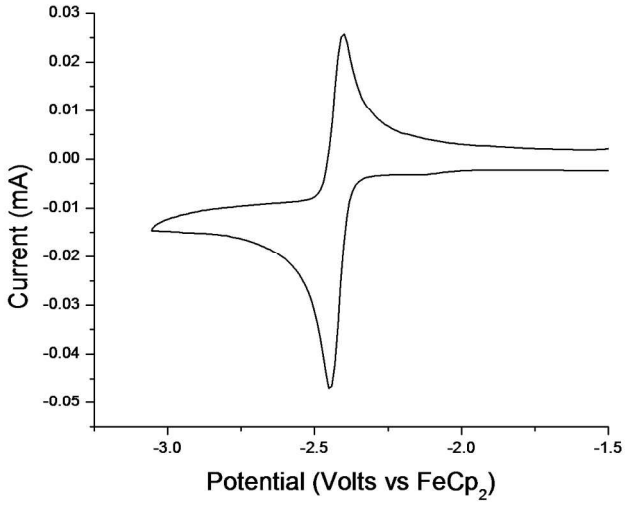

Figure 22. Cyclic voltammogram of 1 mM $[Rh(P^{Ph}{}_2N^{Bn}{}_2)_2]BF_4$ (**2**). Conditions: 0.2 M NBu_4PF_6 in acetonitrile, glassy carbon working and counter electrodes, 100 mV/s scan rate.

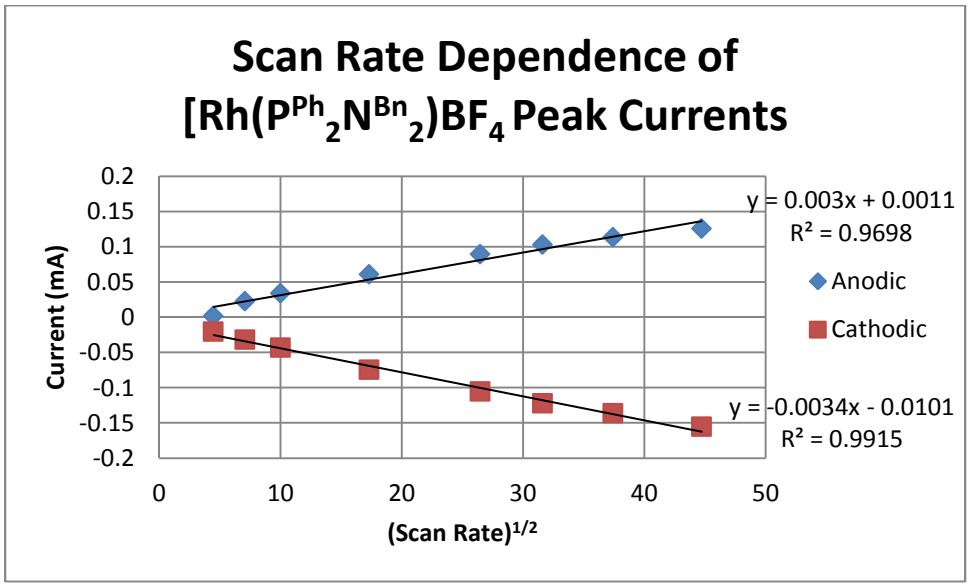

Figure 23. Scan rate dependence study carried of the Rh(1/-1) couple 1 of mM $[Rh(^{Pn}{}_2N^{Bn}{}_2)_2]BF_4$ (**2**). Conditions: 0.1 M NBu_4PF_6 in acetonitrile, glassy carbon working and counter electrodes.

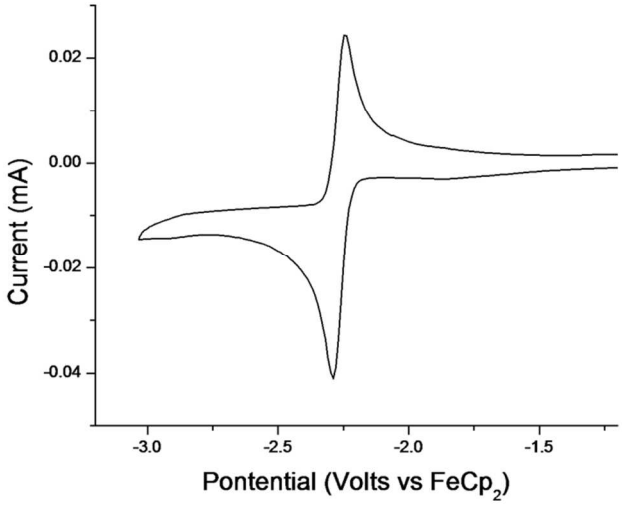

Figure 24. Cyclic voltammograms of 1 mM $[Rh(P^{Ph}{}_2N^{PhOMe}{}_2)_2]BF_4$ (**3**). Conditions: 0.2 M NBu_4PF_6 in acetonitrile, glassy carbon working and counter electrodes, 100 mV/s scan rate.

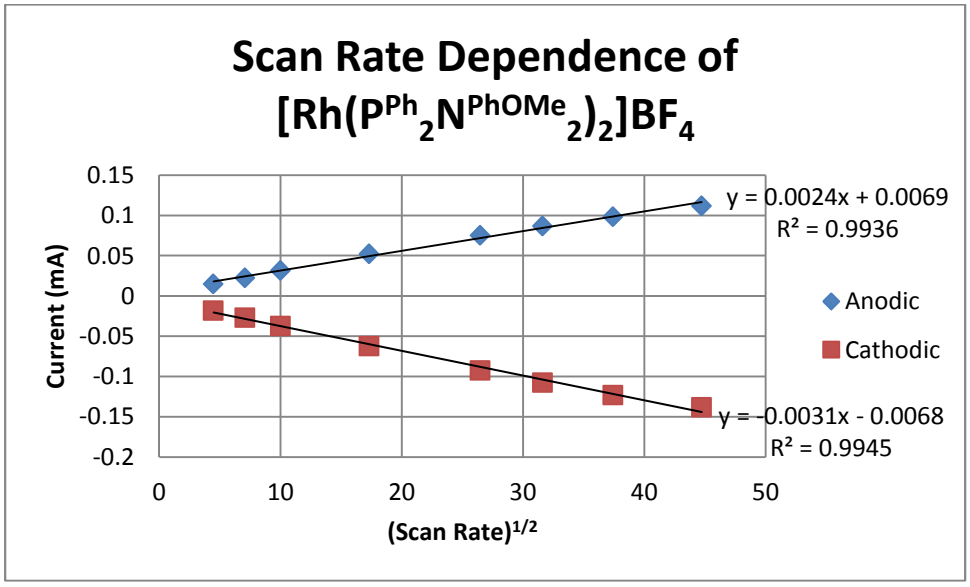

Figure 25. Scan rate dependence study of the Rh(1/-1) couple of 1 mM $[Rh(^{Pn}{}_2N^{PhOMe}{}_2)_2]BF_4$ (**3**). Conditions: 0.1 M NBu_4PF_6 in acetonitrile, glassy carbon working and counter electrodes.

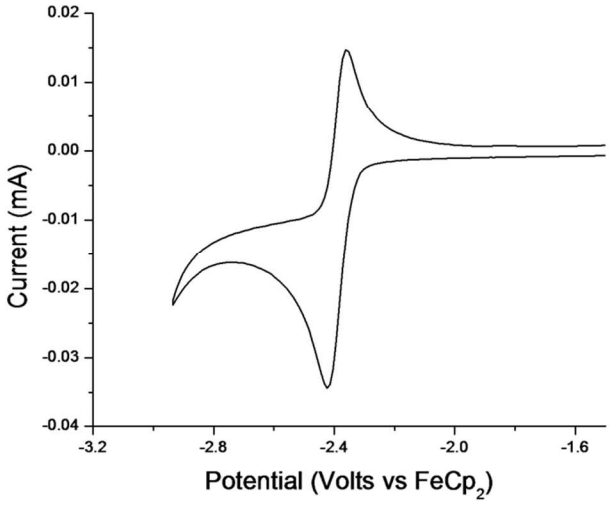

Figure 26. Cyclic voltammograms of 1 mM $[Rh(P^{Cy}_2N^{Ph}_2)_2]BF_4$ (**4**). Conditions: 0.2 M NBu_4PF_6 in acetonitrile, glassy carbon working and counter electrodes, 100 mV/s scan rate.

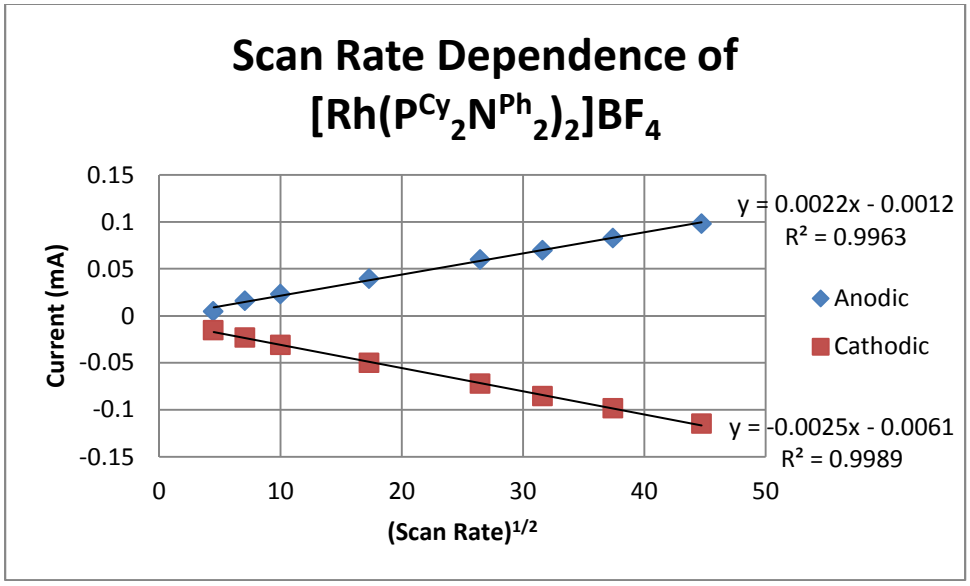

Figure 27. Scan rate dependence study of the Rh(1/-1) couple of 1 mM $[Rh(^{Cy}_2N^{Ph}_2)_2]BF_4$ (**4**). Conditions: 0.1 M NBu_4PF_6 in acetonitrile, glassy carbon working and counter electrodes.

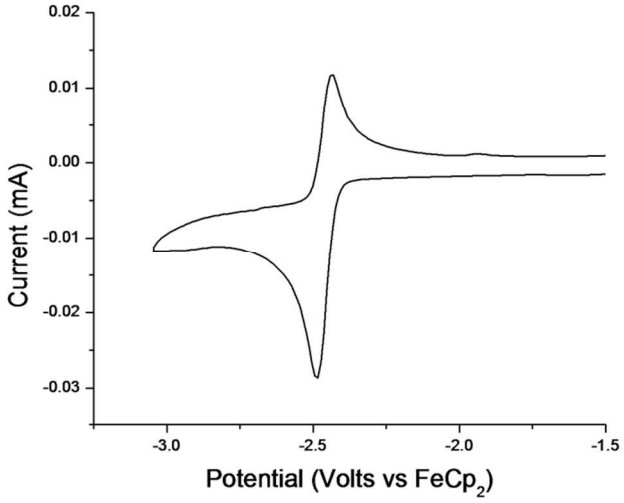

Figure 28. Cyclic voltammograms of 1 mM $[Rh(P^{Cy}_2N^{PhOMe}_2)_2]BF_4$ (**5**). Conditions: 0.2 M NBu_4PF_6 in acetonitrile, glassy carbon working and counter electrodes, 100 mV/s scan rate.

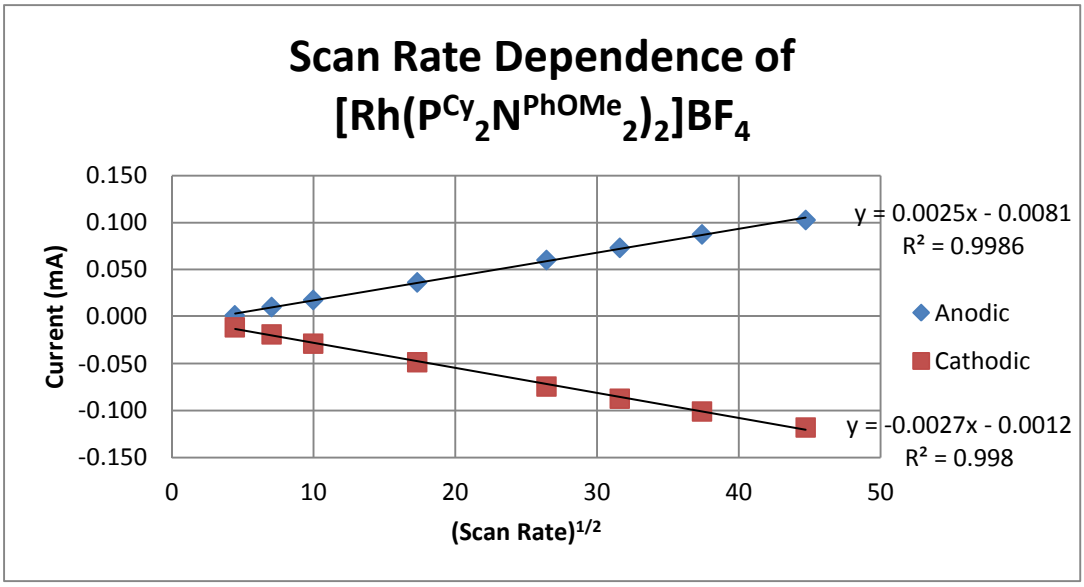

Figure 29. Scan rate dependence study of the Rh(1/-1) couple of 1 mM $[Rh(P^{Cy}_2N^{PhOMe}_2)_2]BF_4$ (**5**). Conditions: 0.1 M NBu_4PF_6 in acetonitrile, glassy carbon working and counter electrodes.

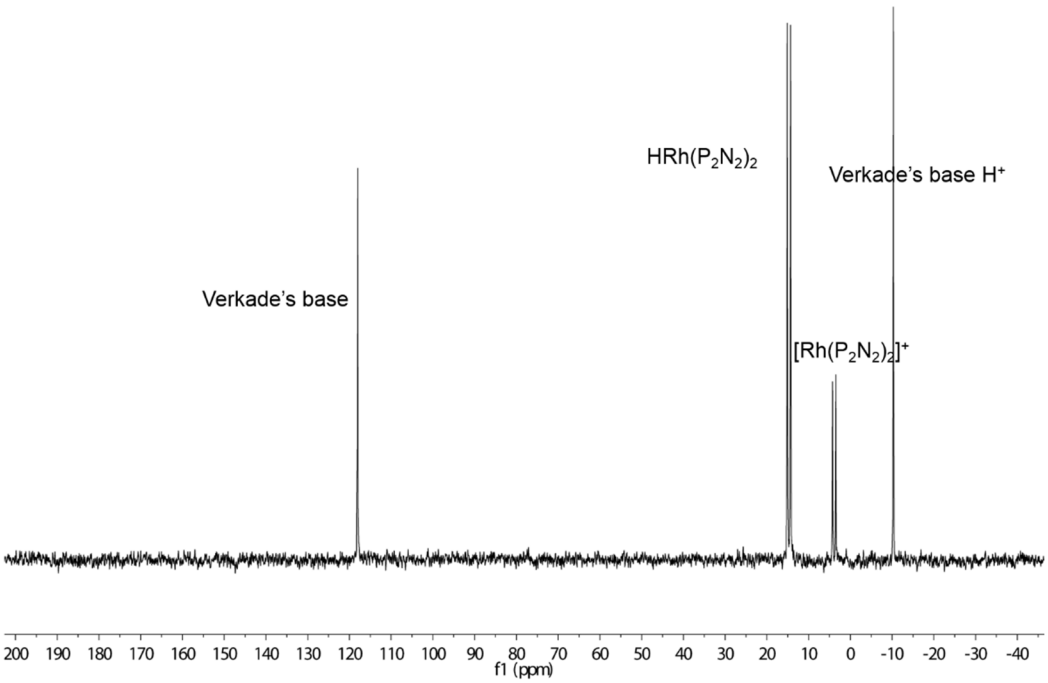

Figure 30. $^{31}P\{^{1}H\}$ NMR of $[Rh(P^{Ph}{}_2N^{PhOMe}{}_2)_2]^+$ (**3**) and Verkade's base under H_2 in benzonitrile showing a typical equilibration reaction.

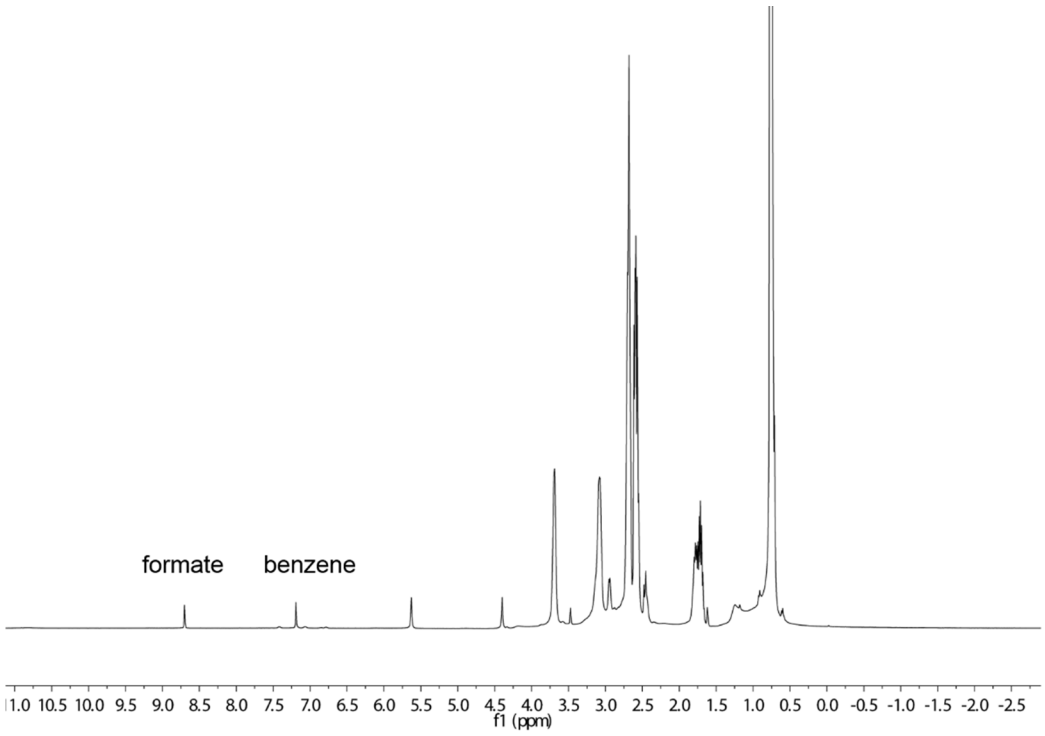

Figure 31. A representative ^{1}H NMR of a catalytic run with $[Rh(P^{Cy}_2N^{Ph}_2)_2]^+$ (**4**).

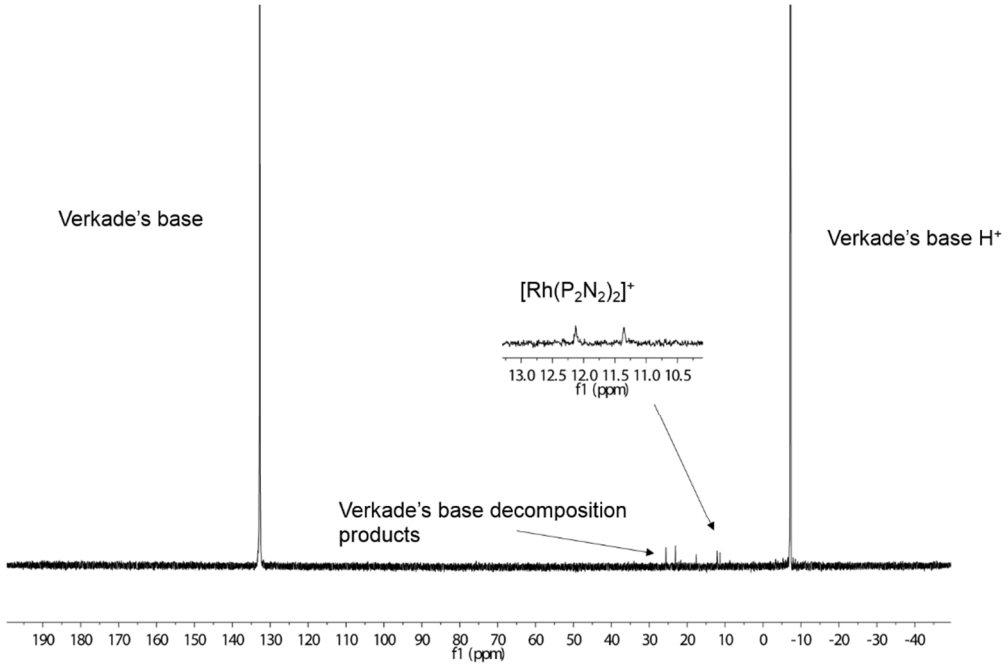

Figure 32. A representative $^{31}P\{^{1}H\}$ NMR of a catalytic run with $[Rh(P^{Cy}_2N^{Ph}_2)_2]^+$ (**4**).

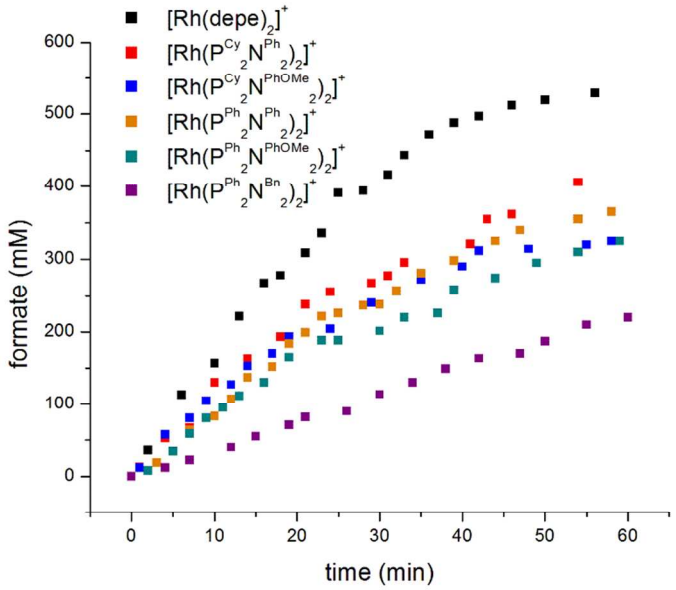

Figure 33. Formate vs time for each metal complex over an hour.

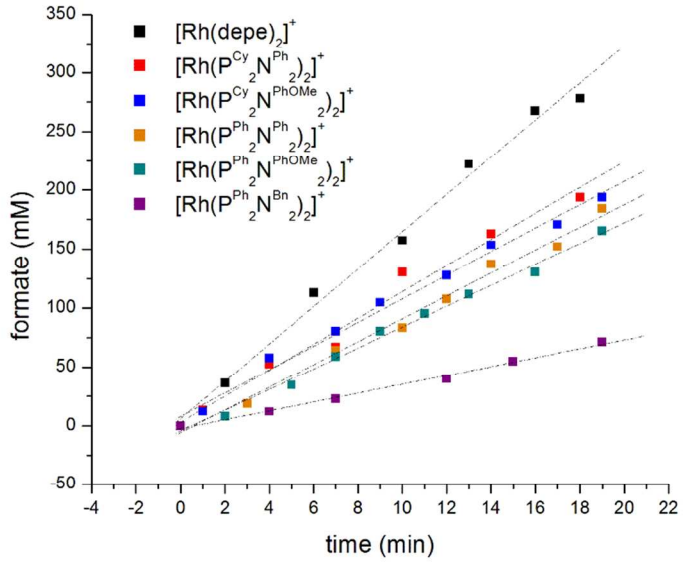

Figure 34. Formate vs time for each metal complex for 20 min showing regions fitted to obtain kinetic rates.